Supplementary Material

Estimating Soil Organic Carbon Stocks of Swiss Forest Soils by Robust External-drift Kriging

Madlene Nussbaum[1], Andreas Papritz[1], Andri Baltensweiler[2], Lorenz Walthert[2]
[1] Institute of Terrestrial Ecosystems (ITES), ETH Zurich, Universitätstrasse 16, CH-8092 Zurich,
[2] Swiss Federal Institute for Forest, Snow and Landscape Research (WSL), Zürcherstrasse 111, CH-8903 Birmensdorf

Contents

Descriptive statistics of calculated SOC stocks

Table 1: Descriptive statistics of SOC stock, calculated for the mineral topsoil (0–30 cm), the mineral soil to 100 cm depth and the subsoil (30–100 cm, cs: calibration set [n = 858], vs: validation set [n = 175], stdv: standard deviation, MAD: median absolute deviation).

	SOC 0–30 cm		SOC 0–100 cm		SOC 30–100 cm	
	cs [kg m^{-2}]	vs [kg m^{-2}]	cs [kg m^{-2}]	vs [kg m^{-2}]	cs [kg m^{-2}]	vs [kg m^{-2}]
minimum	0.83	2.66	0.99	2.80	0.00	0.00
maximum	36.10	22.60	96.39	56.97	63.17	37.27
mean	7.09	8.09	10.89	13.29	3.80	5.20
median	6.09	7.30	8.94	11.18	2.79	3.56
stdv	4.10	4.12	7.25	8.33	4.06	5.16
MAD	3.03	3.45	4.53	6.05	2.14	3.03

Information on covariates representing parent material and soil

Table 2: Description of map units used to represent parent material and pedogenetic conditions. The physiogeographic units A–Z of the soil map (SM, map scale 1:200 000, Swiss Federal Statistical Office, 2000a) were intersected with selected polygons of the Geological Map of Switzerland (GM, map scale 1:500 000, Swisstopo, 2005) and with units of the maps of the Last Glacial Maximum (LGM, map scale 1:500 000, Swisstopo, 2009) and of the Biogeographic Subregions (Gonseth *et al.*, 2001).

Label	Description
A	Tabular Jura
B	Basins and valleys in Haute Chaine and Tabular Jura
C	Elongated valleys in Haute Chaine Jura
D	Plateau Jura
E	Ridges in Haute Chaine Jura
F	Plains on lower Central Plateau
G	Moraine hills
H	Lower Molasse hills partly covered by moraines
J	Fluvial valleys on Central Plateau
K	Molasse hills at intermediate altitude partly shaped by glaciers
L	Drumlin landscapes with marked relief
M	Higher Molasse hills with marked relief shaped by erosion (Hörnli)
N	Higher Molasse hills with marked relief shaped by erosion (Napf)
O	Northern Alpine foothills consisting predominantly of sandy Molasse
P	Northern Alpine foothills consisting predominantly of Molasse conglomerates
Q	Wide Alpine valleys
R	Narrow Alpine valleys
S	Alpine Flysch and Bündner slate, mainly within the Northern Alps
T	Alpine Bündner slate in the upper Rhone valley and Ticino
U	Alpine limestone mountains
V	Alpine mountains of crystalline basement consisting of hard rocks
W	Alpine mountains of crystalline basement consisting of easily weatherable rocks
X	Southern Alpine foothills consisting of Molasse sediments and partially covered by moraines
Y	Fluvial valleys in Ticino
Z	Plains of Magadino and Mendrisio
Additionally created units:	
FLY	Flysch formations tending to form wetlands (GM units ’ha’,’hd’,’hj’,’ie’,’ja’,’jd’,’jc’)
DEC	Old fluvioglacial gravel-rich terraces dominantly with strongly acid soils (GM unit ’an’ within SM units F, G, H, P, A, E and J)
MOR	Old glacial till and moraines dominantly with strongly acid soils (GM unit ’al’ outside LGM)
MOW	Younger glacial drift with less acid soils (GM unit ’al’ within LGM)
Uv	Permian sand stones (Verrucano) often carrying podzols, but intermingled with otherwise calcareous soils (GM units ’jo’, ’fq’ and ’fp’ within SM unit U)
Vsa	SM unit V within the Biogeographic Subregion SA1 (Southern Alps including Poschiavo and Val Bregaglia)
Vst	SM unit V within the Biogeographic Subregion SA2 (Southern Ticino)
Wsa	SM unit W within the Biogeographic Subregion SA1
Wst	SM unit W within the Biogeographic Subregion SA2

Evolution of root mean squared error in model building

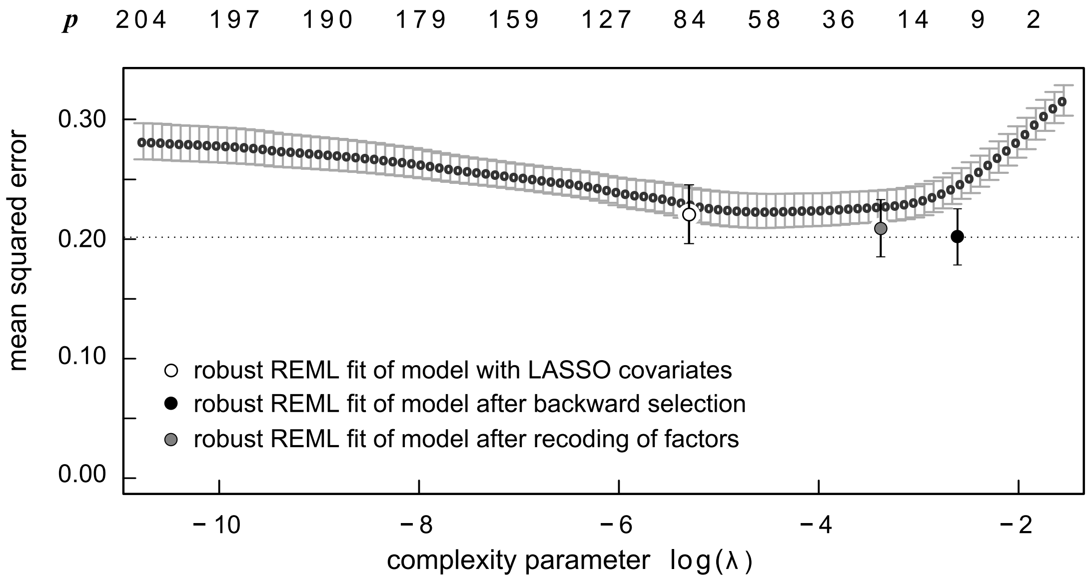

Figure 1: Mean squared errors (MSE) plotted against the complexity of the model for SOC stock in 0–100 cm depth. Shown are MSE of the complete LASSO selection path and of the robust REML model fits after model reduction by LASSO, backward selection by tenfold cross validation and of the final model after aggregating levels of categorical covariates (p: number of covariates in model). The vertical bars give the standard errors computed from the 10 cross-validation subsets.

Estimated parameters of final models for SOC stocks

Table 3: Regression coefficients β and standard errors (SE) for each covariate used in the final model for prediction of SOC stock in 0–30 cm. Soil map units (factor with 34 levels, see Table 2) encoded as treatment contrasts with first level of categorical covariate as reference. TPI500: topographic position index (Jenness, 2006) with radius of 500 m.

Covariate		β	SE
Intercept		4.1220	0.2317
Mean annual precipitation (square root) [mm]		0.0109	0.0014
Reflection in near-infrared band of SPOT5 mosaic [%]		-0.0011	0.0034
TPI500 for soil map units rich in clay (SM units A, E, FLY) [m]		-0.0018	0.0005
TPI500 for soil map units poor in clay (remaining SM units) [m]		0.0029	0.0001
Mass of soil particles < 2 mm assigned to geotecnical map units [0.1 kg m^{-2}]		-0.0003	0.0001
Soil map units	A, E, FLY, Vst, Wsa, Wst (reference units)	0.0000	
	B, C, D, G, F, H, L, K, M, N, MOW, MOR, DEC	-0.3770	0.0623
	J, Q, O, P, V, W, X, Y, Z, Vsa	-0.4978	0.0574
	R, S, T, U	-0.2596	0.0555

Table 4: Regression coefficients β and standard errors (SE) for each covariate used in the final model for prediction of the SOC stock in 0–100 cm. Soil map units (Table 2) encoded as treatment contrasts with unit A as reference.

Covariate		β	SE
Intercept		3.8429	0.2244
Mean March precipitation (square root) [mm]		0.0336	0.0049
Reflection in near-infrared band of SPOT5 mosaic [%]		-0.0094	0.0036
Slope angle (resolution 2 m) [°]		0.0037	0.0017
Soil map units	A (reference unit)	0.0000	
	B, C, D, G, F, H, L, V, Y, MOR, MOW, DEC	-0.2740	0.1440
	E, FLY, Vsa,Wsa, Wst	0.1761	0.1504
	J, Q, O, P, X, Z	-0.4165	0.1501
	K	-0.3772	0.1589
	M, N	-0.2905	0.1744
	R, S, T, U, W	-0.0754	0.1466
	Uv	-1.1397	0.2262
	Vst	0.5959	0.1695

Table 5: The estimated parameter of the exponential variograms fitted for the final models for SOC stocks in 0–30 and 0–100 cm show weak spatial autocorrelation. For both models an effective range of about 600 m was fitted.

	nugget τ^2 [(log(kg m^{-2}))^2]	sill σ^2 [(log(kg m^{-2}))^2]	range α [m]
0–30 cm	0.0008	0.0013	203.6
0–100 cm	0.0009	0.0013	211.1

Partial residual plots for covariates of final models

The partial residual plots (e.g. Faraway, 2005, p. 72) in Figures 2 and 3 reflect the positive coefficients of precipitation by ascending and the negative coefficients of near-infrared reflectance by descending curves (solid line). The partial residuals of the soil map units (panel f in Figure 2 and d in Figure 3) show large SOC stocks for map units belonging to the Jura mountains with dominantly calcareous soils (A, E), the Flysch formations (FLY), both rich in clay, and the Southern Alps (Wsa, Wst, Vsa, Vst). Very small SOC stocks were found on Permian Verrucano (Uv).

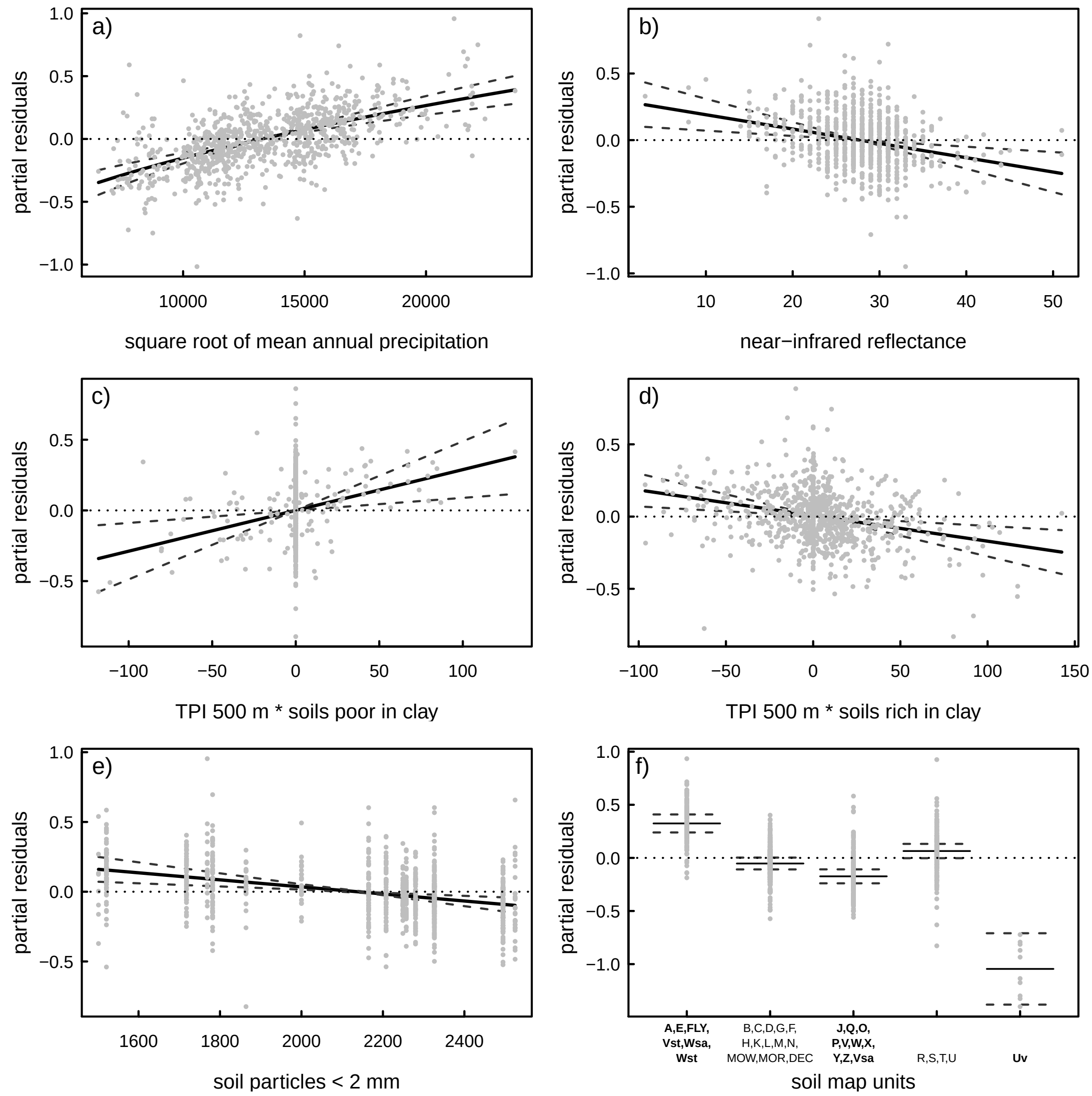

Figure 2: Partial residual plots for each covariate of the final model for prediction of the SOC stock in 0–30 cm depth (TPI500: topographic position index with radius of 500 m [> 0 for mounds and < 0 for depressions]; solid lines: fitted coefficient; dashed lines: fitted coefficients ± SE, see Table 2 for an explanation of the labels of the soil map units).

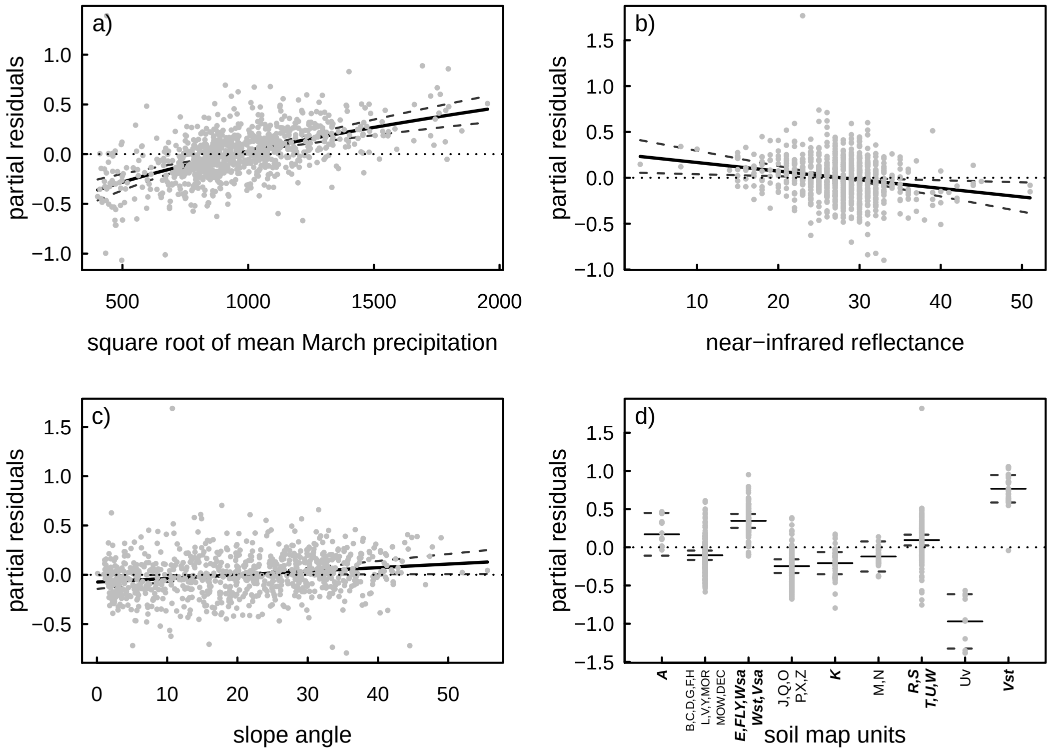

Figure 3: Partial residual plots for each covariate of the final model for prediction of the SOC stock in 0–100 cm depth. (solid lines: fitted coefficient; dashed lines: fitted coefficients ± SE, see Table 2 for an explanation of the labels of the soil map units).

Monte-Carlo approximation of the lognormal block kriging variance

To approximate $\mathrm{Var}[S(B_k) - \tilde{S}(B_k)]$ (equation 11 in main article), we selected i) n_k of the N_k nodes of the 100-m grid falling into region B_k, or ii) all N_k grid nodes discretizing the forest area of Switzerland randomly without replacement and computed for each such sample the approximation

$$\begin{aligned}\mathrm{Var}[S(B_k) - \tilde{S}(B_k)] \approx {} & \frac{1}{N_k^2} \sum_{\boldsymbol{s}_i \in B_k} \mathrm{Var}[S(\boldsymbol{s}_i) - \tilde{S}(\boldsymbol{s}_i)] \\ & + \frac{N_k - 1}{N_k\, n_k\, (n_k - 1)} \sum_{\boldsymbol{s}_i \in \text{sample}} \;\sum_{\boldsymbol{s}_j \in \text{sample},\, \boldsymbol{s}_j \neq \boldsymbol{s}_i} \mathrm{Cov}[S(\boldsymbol{s}_i) - \tilde{S}(\boldsymbol{s}_i), S(\boldsymbol{s}_j) - \tilde{S}(\boldsymbol{s}_j)].\end{aligned} \tag{1}$$

For the ecoregions, we computed the above expression for 1 000 independently chosen samples, each sample consisting of $\max(0.01\, N_k, 500)$ nodes in B_k, and approximated $\mathrm{Var}[S(B_k) - \tilde{S}(B_k)]$ by their mean.

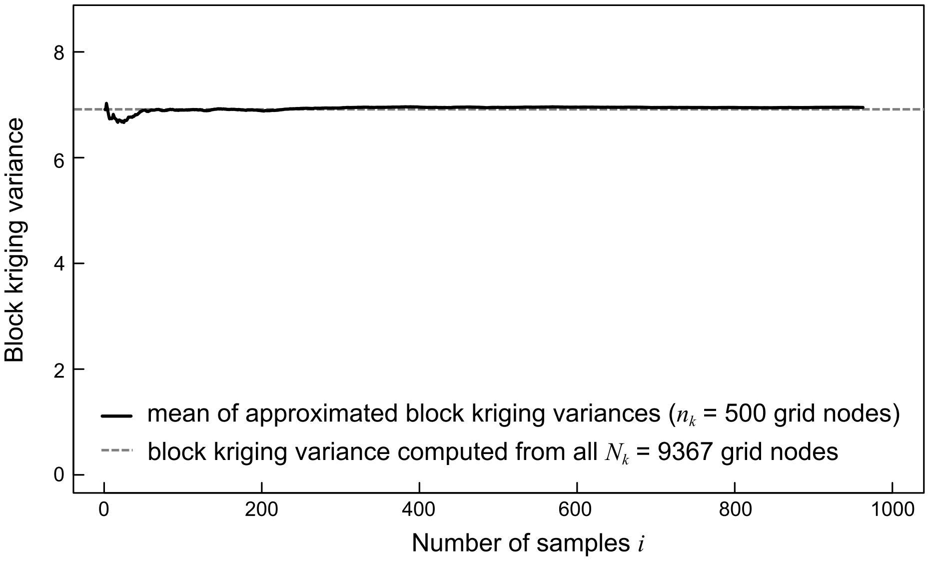

Figure 4: Mean (averaged up to i samples) of approximated block kriging variances computed each by equation 1 for random samples of size $n_k = 500$ (solid line) and value of block kriging variance computed directly by equation equation 11 in main article for stratum Alps ≤600 m ($N_k = 9\,367$ grid nodes, grey dashed line).

To predict the mean stocks for whole Switzerland, we averaged the approximations for 2 000 samples, each sample consisting of about 5 500 randomly chosen grid nodes. Figure 4 shows that the Monte-Carlo approximation is excellent for a region with 9 367 grid nodes, for which we could evaluate equation 11 in main article directly. In equation 1 the covariance between the lognormal point prediction errors at two locations $\boldsymbol{s}_i$ and $\boldsymbol{s}_j$ was computed by

$$\begin{aligned}\mathrm{Cov}[S(\boldsymbol{s}_i) - \tilde{S}(\boldsymbol{s}_i), S(\boldsymbol{s}_j) - \tilde{S}(\boldsymbol{s}_j)] = \mu_{\hat{\theta}}(\boldsymbol{s}_i)\,\mu_{\hat{\theta}}(\boldsymbol{s}_j)\Big\{&\exp\Big(\mathrm{Cov}[Y(\boldsymbol{s}_i), Y(\boldsymbol{s}_j)]\Big)\\ &- \exp\Big(\mathrm{Cov}[Y(\boldsymbol{s}_i), \tilde{Y}(\boldsymbol{s}_j)]\Big) - \exp\Big(\mathrm{Cov}[\tilde{Y}(\boldsymbol{s}_i), Y(\boldsymbol{s}_j)]\Big)\\ &+ \exp\Big(\mathrm{Cov}[\tilde{Y}(\boldsymbol{s}_i), \tilde{Y}(\boldsymbol{s}_j)]\Big)\Big\}\end{aligned} \qquad (2)$$

with $\mu_{\hat{\theta}}(\boldsymbol{s}_i)$ (and $\mu_{\hat{\theta}}(\boldsymbol{s}_j)$ analogously) approximated by

$$\mu_{\hat{\theta}}(\boldsymbol{s}_i) \approx \exp\left(\boldsymbol{x}(\boldsymbol{s}_i)^{\mathrm{T}}\hat{\boldsymbol{\beta}}_{\hat{\theta}} + 1/2\,(\hat{\tau}^2 + \hat{\sigma}^2)\right).$$

$\mathrm{Cov}[Y(\boldsymbol{s}_i), Y(\boldsymbol{s}_j)]$ can be computed from the estimated variogram, exploiting the well-known relation between a weakly stationary variogram and an autocovariance function (e.g. Diggle and Ribeiro, 2007, p. 47), and the remaining covariance terms are given by

$$\mathrm{Cov}[\tilde{Y}(\boldsymbol{s}_i), \tilde{Y}(\boldsymbol{s}_j)] = \left(\boldsymbol{\gamma}_{\hat{\theta}}(\boldsymbol{s}_i)^{\mathrm{T}}\,\boldsymbol{\Gamma}_{\hat{\theta}}^{-1}, \boldsymbol{x}(\boldsymbol{s}_i)^{\mathrm{T}}\right)\ \mathrm{Cov}\left[\begin{pmatrix}\hat{\boldsymbol{Z}}\\ \hat{\boldsymbol{\beta}}\end{pmatrix}, \left(\hat{\boldsymbol{Z}}^{\mathrm{T}}, \hat{\boldsymbol{\beta}}^{\mathrm{T}}\right)\right]\begin{pmatrix}\boldsymbol{\Gamma}_{\hat{\theta}}^{-1}\,\boldsymbol{\gamma}_{\hat{\theta}}(\boldsymbol{s}_j)\\ \boldsymbol{x}(\boldsymbol{s}_j)\end{pmatrix}, \qquad (3)$$

$$
\begin{aligned}
\operatorname{Cov}[\tilde{Y}(\boldsymbol{s}_i), Y(\boldsymbol{s}_j)] &= \left(\boldsymbol{\gamma}_{\hat{\theta}}(\boldsymbol{s}_i)^{\mathrm{T}}\, \boldsymbol{\Gamma}_{\hat{\theta}}^{-1},\ \boldsymbol{x}(\boldsymbol{s}_i)^{\mathrm{T}}\right) \operatorname{Cov}\left[\begin{pmatrix} \hat{\boldsymbol{Z}} \\ \hat{\boldsymbol{\beta}} \end{pmatrix}, Y(\boldsymbol{s}_j)\right] \\
&= b\left(\boldsymbol{\gamma}_{\hat{\theta}}(\boldsymbol{s}_i)^{\mathrm{T}}\, \boldsymbol{\Gamma}_{\hat{\theta}}^{-1},\ \boldsymbol{x}(\boldsymbol{s}_i)^{\mathrm{T}}\right) \boldsymbol{M}^{-1} \begin{pmatrix} \boldsymbol{\gamma}_{\hat{\theta}}(\boldsymbol{s}_j) \\ \boldsymbol{X}^{\mathrm{T}} \boldsymbol{\gamma}_{\hat{\theta}}(\boldsymbol{s}_j) \end{pmatrix}, \qquad (4)
\end{aligned}
$$

where b, $\boldsymbol{X}$, $\boldsymbol{M}$ and the covariance matrix of $(\hat{\boldsymbol{Z}}_{\hat{\theta}}^{\mathrm{T}}, \hat{\boldsymbol{\beta}}_{\hat{\theta}}^{\mathrm{T}})$ are as in Künsch *et al.* (2011).

Validation of prediction uncertainty

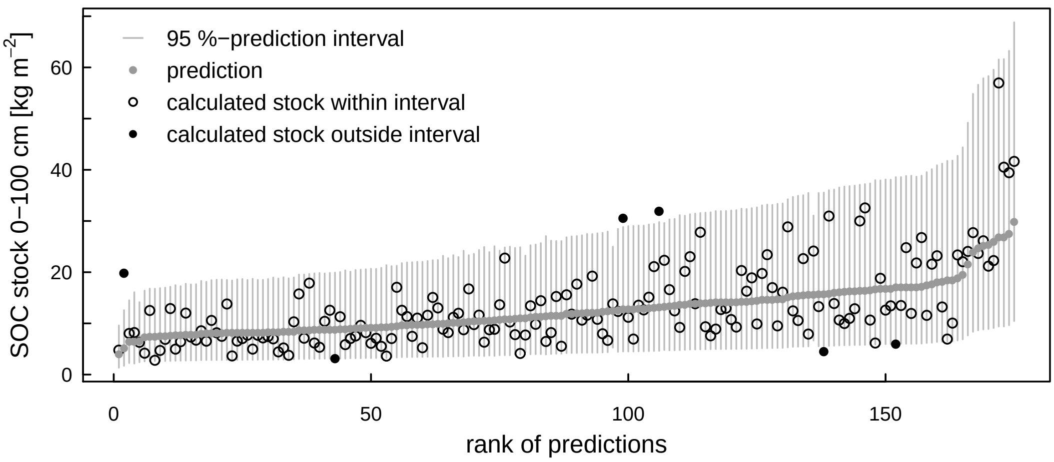

Figure 5: Ranked predictions of the SOC stock down to 100 cm depth of the mineral soil for the 175 sites of the validation set, along with 95 %-prediction intervals (vertical grey lines). Calculated stocks inside the intervals are plotted by open circles, those outside by dark filled symbols.

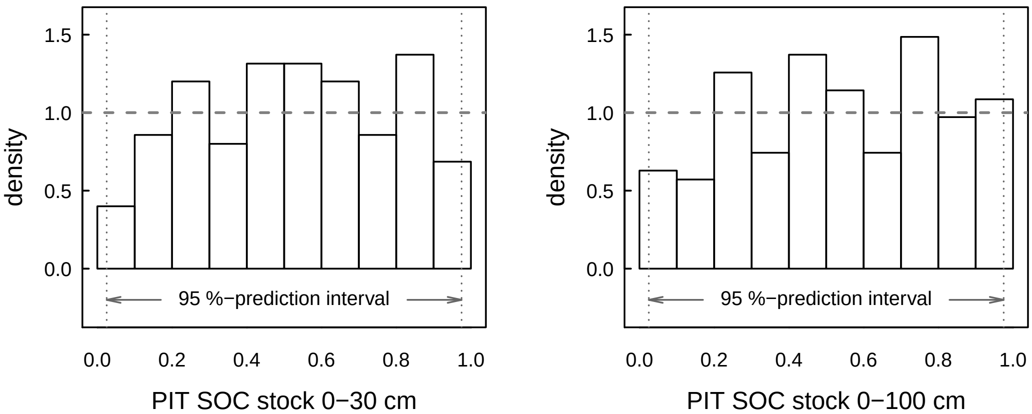

Figure 6: Histograms of probability integral transform (PIT, Gneiting *et al.*, 2007) computed for the calculated SOC stock of the validation set (n = 175). The convex shape of the histograms indicates slight overestimation of prediction uncertainty.